Nisar S, et al., J Food Sci Nutr 2018, 4: 032
DOI: 10.24966/FSN-1076/100032

HSOA Journal of Food Science and Nutrition

Research Article

Gold Nanopellets a Unique Platform for Electrochemical Ultra-Low Detection of Ochratoxin A

Sumaya Nisar, Aakshi Jairath and Tinku Basu*

Amity Institute of Nanotechnology, Amity University Uttarpradesh, Noida, Uttar Pradesh, India

Abstract

Anisotropic nano structures offer exceptional optoelectronic properties when contrasted with isotropic elements and discover application in therapeutics and molecular imaging separated from opto electronic gadgets. Attributable to remarkable optical properties, it is not exploited in electrochemistry up to the fullest extent. The present paper portrays the manufacture of an electrochemical transducer where Gold Nano Pellet (AuNPl) is permitted to develop directly on Indium Tin Oxide (ITO) covered glass electrode utilizing seed-mediated and template free approach which in turn is connected to create Ochratoxin A (OTA) immunosensor (BSA/aOTA/Cys/AuNPl/ITO). The structural and morphology of the proposed electrode are researched utilizing UV-Visible spectroscopy, Cyclic Voltammetry, EDAX, FESEM and AFM. The manufacturing procedure and sensing characteristics of OTA immunosensor are examined utilizing Cyclic Voltammetry (CV). Under optimum experimental conditions, the straight range created by the immunoelectrode is observed to be as 1-20pg mL^{-1}. The LOD and sensitivity of the immunoelectrode are recorded as 0.6pg mL^{-1} and 2.89 × 105Apg^{-1} $mLcm^{-2}$, individually. Ultralow sensing and high sensitivity can be ascribed to high conductivity of AuNPl/ITO electrode and low loading of monoclonal anti Ochratoxin A (aOTA). Least interference is seen in spiked coffee tests due to monoclonal aOTA. The created transducing platform demands a potential application in electrochemical ultra low detection of toxins.

Keywords: Gold nano pellet; Immunosensor; Ochratoxin A; Pico gm; Ultra low detection

Introduction

Extensive insight over knowledge of a nanomaterial is a fundamental factor in building of later and present day gadgets with required functions. Because of this reason, much attention has been committed for outlining of materials in nano administration with complex shapes. Anisotropic nanomaterials are bearing ward showing startling highlights contrasted with isotropic particles to an outstanding degree with applications in numerous devices. Having diverse surface territory and crystallographic facets, anisotropic nanostructures offer highly tunable optical, optoelectronic, electrochemical and magnetic properties as for viewpoint proportion and shape. In the bunch of anisotropic nano structures, gold nanoparticles assume a pivotal role due to its unique shape dependent electron or hole confinement, surface plasmon, tunable electron transfer kinetics, biocompatibility and find enormous application in catalysis, molecular recognition, diagnostics, imaging and therapeutics.

The variation in longitudinal wave in nanobelts, nanocombs [1], nanotubes or nanowires [2], of gold like other noble metals showcase outstanding electro catalytic activities, magical detecting capacity to trace biomolecule with enhanced sensitivity [3,4], imaging of *Bacillus subtilis* spores (a simulant of *Bacillus anthracis*) utilizing Two-Photon Radiance (TPR) microscopy [5], and recognizing ability of heavy metals for example, Cu^{2+} and Hg^{2+} ions [2], and so forth. The sensing ability of anisotropic nano structured gold is fundamentally limited to optical gadgets programmed on fluorescence, SERS and surface plasmon resonance [2]. Investigation on anisotropic nano sized gold as an electrochemical detecting framework is yet to be investigated. Few illustrations such as bimetallic Au-Pt nanowires for continuous no enzymatic impedimetric sensing of glucose [2,6], and one dimensional Gold Nanostructure (AuNs) relied upon thiol functionalized Graphene Oxide (GO-SH) for identification of free cholesterol up to a level of 0.2nM within 5 seconds and so on [7], can be referred to.

Mutagenic and cancer-causing mycotoxins, for example, aflatoxins, sterigmatocysin, ochratoxins or fuminisin contaminate the food chain and impose a serious medical problem for both the animal and plant species [6]. Among every one of the mycotoxins, nine number of Ochratoxins have been recognized till date with Ochratoxin A (OTA) being one of the most pervasive and perilous mycotoxins and has received widespread attention in regards to the food pollution and safety [8,9]. It is recognized as a significant nephrotoxic, teratogenic, cancer-causing and immunosuppressive operator which significantly influences the animal, generally rodent, mice and other mammalian

***Corresponding author:** Tinku Basu, Amity Institute of Nanotechnology, Amity University Uttarpradesh, Noida, Uttar Pradesh, India, Tel: +91 1204392510; E-mail: tbasu@amity.edu

Citation: Nisar S, Jairath A, Basu T (2018) Gold Nanopellets a Unique Platform for Electrochemical Ultra-Low Detection of Ochratoxin A. J Food Sci Nut 4: 032.

Received: April 15, 2018; **Accepted:** June 07, 2018; **Published:** June 21, 2018

species. Studies have demonstrated that OTA at cell level outcomes in expanded oxidative stress and abnormal state of the poison in people causing "Balkan endemic nephropathy". Numerous nations over the globe have set regulatory levels for the usage of OTA depending on the food commodities consumed [8,10]. Among all the countries, Europe is known to be a prolific consumer of the OTA-contaminated foods and the European Union has fixed the amount of OTA to be permitted in the food items which is 5ppb for crude grains, 2ppb for wines and 0.5ppb for child nourishments (Commission Regulation No. 123/2005) [8]. Usually, OTA is found in minute amount starting from nanograms to micrograms per gram of the food product. Subsequently, modern instrumental investigation, for example, High-Performance Liquid Chromatography (HPLC) or Gas Chromatography (GC) coupled to ultraviolet-visible, fluorescence or mass spectrometry [11], and molecular recognition element such as Enzyme-Linked Immunosorbent Assay (ELISA) are investigated to detect OTA precisely and particularly in the food products [12]. Attributable to high cost, need of sophisticated research laboratory and trained manpower, complex sample preparation steps, and lacking of exactness in the ultra low detection range, these instruments are not really used to detect OTA in the natural way of life unless it is compulsory which brings about constant intake of OTA contaminated food causing serious and interminable effects in animal and human health. This could raise the need of developing reliable, smart, portable, rapid and cost effective sensing tool for checking of OTA in food items.

In the past years, biosensors have emerged as an exceptionally assertive alternative to the conventional analysis protocols because of its high sensitivity, selectivity, technical simplicity, and portability [13,14]. Studies reveal that electrochemical (amperometric and impedimetric) biosensors are the most popular one due to low cost, ease of operation, direct measurement, high sensitivity, fast response time and ease of scale up as compared to piezoelectric or optical biosensors [15]. The last decade has seen the development of many immunosensors for the detection of OTA based on the strong interaction between the antibody-antigen [16]. Vidal et al., have demonstrated a labeled electrochemical immunosensor for OTA detection within wide range of (10^{-4} to 1000ng mL^{-1}) on Screen Printed Electrode (SPE). They have employed an OTA-peroxidase enzyme conjugate and magnetic bead for signal amplification. Radi et al., have reported a label-free electrochemical impedimetric immunosensor for detection of OTA with a detection limit of 0.5ng mL^{-1} [17]. The Electrostatic Impedance Spectroscopy (EIS) has resulted in a linear relationship between the charge transfer resistance and the concentration of OTA within a range of 1-20ng mL^{-1}. Electrochemical enzyme linked Immunosorbent assays based on screen printed electrodes have been developed by Alarcon et al., for the rapid detection of OTA in wheat with a detection limit of 0.4µg/kg and this method uses the samples directly with the assay without any clean-up [18]. Zamfir et al., have developed a label-free immunosensor based on Magnetic Nanoparticles (MNPs) for high selectivity of OTA [19]. Ngundi et al., have proposed an array biosensor based on competitive immunoassay format for the detection of OTA in cereals and beverages and achieved a detection limit of 3.8 to 100ng g^{-1} for cereals and a LOD between 7 to 38ng g^{-1} for coffee and wine [20]. Development of OTA biosensor using OTA specific aptamer has been extensively investigated [21,22]. The investigation on OTA biosensor highlights couple of vital confinement, for example, limit recognition run, low affectability, poor time span of usability, detection limit. The inspiration for the present examination is to build up a mark free direct immunosensor for ultra Low Recognition Limit (LOD) of OTA.

In the present investigation, anti OTA immobilized on thiol functionalized gold nano pellet, as grown directly on Indium Tin Oxide coated glass sheet (ITO) is employed to detect OTA up to a level of 0.6pg mL^{-1}. The nano Gold Pellets (AuNPl) are grown on ITO surface using Au seeds, ascorbic acid and CTAB [23-26]. The fabricated AuNPl/ITO electrode is functionalized with cystamine to impart amine moieties on the surface. Further this functionalized electrode is allowed to bioconjugated with activated monoclonal antibodies of OTA (aOTA). The fabricated immunoelectrode is designated as BSA/aOTA/Cys/AuNPl/ITO is used to recognize OTA in spiked coffee samples.

Materials and Methods

Chemicals and reagents

Aurochloric acid ($HAuCl_4$), trisodium citrate, Sodium borohydride ($NaBH_4$), (3-Aminopropyl) tri-methoxysilane (APTMS), ascorbic acid, Cetyltrimethyl ammonium bromide (CTAB), (3-Dimethylaminopropyl) N-ethylcarbodiimide hydrochloride (EDC), N-Hydroxysuccinimide (NHS), cystamine (Cys), Ochratoxin A (OTA), monoclonal anti-Ochratoxin A (aOTA) were purchased from Sigma-Aldrich. Hydrochloric acid (HCl) and Methanol were purchased from Merck and Co, USA. Deionized water (18MΩcm) was used for the preparation of solutions.

Instrumentation

Cyclic voltammetry studies were carried out via Autolab Potentiostat/Galvanostat Model AUT83945 (PGSTAT302N) using the conventional three-electrode system. BSA/aOTA/Cys/AuNPl/ITO, as the working electrode, platinum wire (Pt) as the auxiliary electrode, and saturated Ag/AgCl as the reference electrode was used in PBS (50mM, pH 7.0, 0.9% NaCl) containing 5mM $[Fe(CN)_6]^{3-/4-}$ as a redox mediator. The surface morphology was studied by field emission scanning electron microscope (FE-SEM: MIRA II LMH) and atomic force microscope (NDMT) and elemental analysis were done using energy dispersive X-ray diffraction (INCA Penta FET3). UV-vis spectra were measured using Hitachi U3300 spectrophotometer.

Solution preparation

The deionized water (18MΩcm) was used for the preparation of buffer solutions. Anti-OTA antibody (40µg mL^{-1}) solution was prepared in 50mM phosphate buffer [(PB), 50mM, pH 7.4] with 10% methanol. A solution of Bovine Serum Albumin (BSA) (1mg mL^{-1}) was prepared in PB (50mM, pH 7.0) and used as the blocking agent for nonspecific binding sites.

Preparation of ITO substrates

ITO glass slides of 0.25cm × 0.25cm were cleaned prior to use. The cleaned and dried substrates were soaked in 10% HCl for 10min. The substrate was annealed at 450°C for 7h and then cooled to room temperature. The substrates were then soaked in 30mM of APTMS solution in methanol for 1h for functionalization. Afterward, they were washed with methanol and water. The substrates were kept at 100°C for 2h. Thus, APTMS treated ITO substrate was prepared.

Fabrication of AuNPl/ITO electrode

Seed mediated growth approach was used to grow Gold Nanopellets (AuNPl) onto the ITO substrate. Gold nano seeds were prepared by adding 0.1M ice cold $NaBH_4$ to 10mM Sodium Citrate and $HAuCl_4$ solution. APTMS functionalized ITO substrate was dipped in the prepared seed solution for 30 minutes and then immersed in a growth solution containing 0.2M CTAB solution, 0.1M AA and 0.01M $HAuCl_4$ for 6h to prepare AuNPl/ITO electrodes. Thus as prepared electrodes were washed three times to get rid of excess CTAB and unreacted reactants.

Fabrication of the OTA immunoelectrode (BSA/aOTA/Cys/AuNPl/ITO)

AuNPl/ITO electrodes were further modified to develop immunoelectrodes. AuNPl/ITO was functionalized with 0.04M Cys to impart amine moieties on to the electrode. The optimized concentration of 40ng mL^{-1} aOTA was used for fabrication of the immunoelectrode. aOTA antibodies were activated using 0.2M EDC and 0.05M NHS for 2h. 10µL of the activated aOTA antibodies are smeared over the electrode and incubated at 4°C for 16h. To block the nonspecific sites of the immunoelectrode 1mg mL^{-1} BSA was used. Thus, BSA/aOTA/Cys/AuNPl/ITO immunoelectrode was fabricated and kept in 4°C until further use.

Detection of OTA

The stock solution of OTA was diluted to make the different concentration of OTA. The excess unbound OTA was removed by washing with PB (pH 7.4). The fabricated immunoelectrode (BSA/aOTA/Cys/AuNPl/ITO) was allowed to interact with different concentrations of OTA and Electrochemical Cyclic Voltammetry (CV) was used for the analysis. Cyclic voltammetry studies were carried out via Autolab Potentiostat/Galvanostat Model AUT83945 (PGSTAT302N) using the conventional three-electrode system. BSA/aOTA/Cys/AuNPl/ITO was used as the working electrode, Platinum wire (Pt) as the auxiliary electrode, and saturated Ag/AgCl as the reference electrode in PBS (50mM, pH 7.0, 0.9% NaCl) containing 5mM$[Fe(CN)_6]^{3-/4-}$ as a redox mediator.

Detection of OTA in spiked coffee extract: OTA was also detected in contaminated coffee samples by manually spiking them with different concentrations of OTA. 2g of ground coffee powder was accurately weighed and the sample was extracted with 10mL of methanol-water (7:3, v/v). The sample was shaked and sonicated in an ultrasound bath for further 35 minutes at room temperature and centrifuged at 6000rpm for 20 minutes. The supernatant was collected and spiked with known concentration (5, 16, 20pg mL^{-1}) of OTA. The spiked samples were tested with the developed immunoelectrode. The testing was repeated thrice. The test results were compared with the actual concentration and relative error was calculated.

Stability studies

The stability studies of the BSA/aOTA/Cys/AuNPl/ITO immunoelectrode were examined at regular interval of 5 days. 30 sets of BSA/aOTA/Cys/AuNP/ITO immunoelectrodes were fabricated and stored at 4°C. The response studies of the electrodes were investigated after every 5 days through CV in PBS (50mM, pH 7.4, 0.9% NaCl).

Results and Discussion

Morphological analysis

Field Emission Scanning Electron Microscopy (FESEM) and Atomic Force Microscopy (AFM) studies of AuNPl/ITO electrodes: Figure 1 shows the surface topography of Au seed and AuNPl/ITO as captured by FESEM image analysis of FESEM. Figure 1a illustrates an uneven, scatter distributed and densely populated Au seeds on ITO. However, figure 1b shows the FESEM image of AuNPl in various shapes and sizes collectively nomenclature as gold nanopellets. Unevenly scattered AuNPl, as seen on ITO surface varies in sizes and shapes with a dominance of cubical shaped pellets with an average edge length of 125nm. AuNPl are successfully grown as randomly arranged asymmetric cluster on the modified ITO surfaces as depicted by FESEM images. Few percentage of Au nanocuboidal pellets are observed with truncated corners and edges, the remaining being tetragonal, pentagonal and hexagonal shape. The shape directing behavior of CTAB is attributed to the (111) facets of Au being strongly adsorbed by the capping agent to promote growth in other crystallographic directions [24]. FESEM image reveals (Figure 1b) that some of the nanocrystals are fused into one another to form dense and extensive network of nanostructures. Chemical deposition studies [2], state when atoms are added to a surface they diffuse until they locate a step site where they can be incorporated. The decrease in bulk energy (favors growth) and the increase in surface energy (favors dissolution) control the comprehensive growth of nanocrystals. Thus, the evolution of seeds to nanocrystals is based on the dynamic interplay between the above two. The variation in shape and dimension are the inherent limitation of soft template approach. Inspite of our best effort to prepare uniform pellet by manipulating the concentration of CTAB and other reactants, growth temperature and deposition time, variation in shape and sizes cannot be avoided. Increasing the growth time to 18h-22h allows the pellets to grow into nanorods but it increases the development time for the electrode and makes it a laborious process. This is a drawback of using soft templates for growing anisotropic nanostructures.

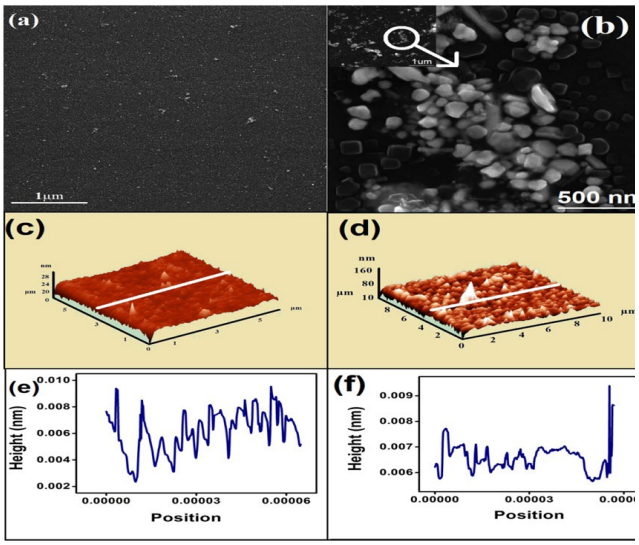

Figure 1: FESEM images of surface morphology of (a) Au seeds. (b) AuNPl in high magnification at 500nm. Inset of (b) shows FESEM image of AuNPl at low magnification of 1µm. AFM images of surface topography. (c) Au seeds for 5µm × 5µm area. (d) AuNP1 for 10µm × 10µm area of developed electrode. Line profile of AFM height image. (e) Au seeds/ITO and (f) AuNP1/ITO.

AFM acts as a standard and reliable tool for knowing the topographical information for the prepared electrode surface particularly at nanometer scale. Figure 1c and 1d illustrate two AFM images of Au seeds and AuNPl/ITO, respectively. The root mean square values of surface roughness obtained for Au seeds and AuNPl are 2.30nm and 8.63nm, respectively. Figure 1c illustrates the scattered and uneven topographical features of Au seeds confirming the deposition of Au seeds onto ITO. These deposited seeds act as platform for the growth of AuNPl on ITO surface as seen in figure 1d. The AFM image of AuNPl/ITO (Figure 1d) shows an asymmetrical and non-homogeneous topographical feature with an average roughness of 6.51nm. Comparatively, the Au seeds have an average roughness of 1.66nm. The upsurge in the surface roughness of AuNPl/ITO as compared to Au seed on ITO accounts the deposition of AuNPl on ITO. The irregularity in the shapes and sizes of AuNPl results a scattered and inconsistent topographical features of AuNPl/ITO as evident from figure 1d. The values of approximate thickness of the Au seed layer assembly and the AuNPl/ITO electrode are 26nm and 90nm respectively as indicated by the height profile of AFM image. The increase in surface thickness of AuNPl layer as compared to seed layer also illustrates the dense population, variation in shapes and sizes of AuNPl (Figure 1e and 1f). The analysis of line profile of Au seed/ITO and AuNPl/ITO clearly shows that AuNPl has higher thickness than Au seed, minimum height as observed on AuNPl/ITO is 6.0nm while minimum height observed for Au seed on ITO is 2.6nm.

UV-Visible spectroscopy and Energy Dispersive Spectroscopy (EDX) studies: Figure 2i demonstrates the UV-Vis spectra for the Au seed/ITO and AuNPl/ITO. The UV-Vis spectra results indicates an absorption band at 525nm (Figure 2ii) for Au seeds which is typical of the plasmon band of AuNPl. Although, the AuNPl exhibits an absorption band at 528nm (Figure 2iii) and only a slight increase in wavelength is seen. This result indicates that the size of the AuNPl formed is altered by the irregular geometry and the concentration of CTAB which acts as a shape directing agent for the nanopellets. However, a drastic increase in absorbance can be seen for the AuNPl nanopellets formed as compared to the Au seeds with not much difference in wavelength.

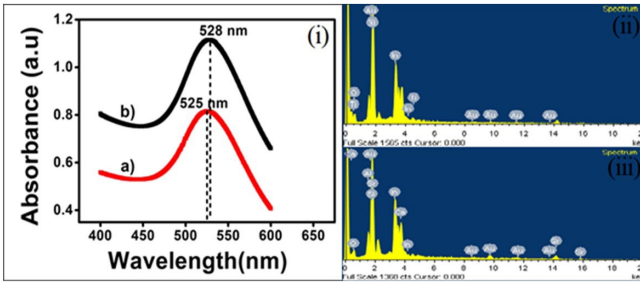

Figure 2: (i) UV-Vis Spectra of a) Au seed and b) Gold nanopellets within 400nm to 650nm and EDX analysis of. (ii) Au seeds/ITO and (iii) AuNPl/ITO.

EDAX was performed to determine the elemental composition of the gold nanopellets which reveals the presence of elemental gold in the Au seeds/ITO and AuNPl/ITO electrode (Figure 2ii and 2iii). A drastic increase is observed in the weight % of pure Au^0 from 6.55% (Au seed/ITO) to 15.95% of (AuNPl/ITO), respectively assuring an enhanced density of pure gold on AuNPl/ITO.

Cyclic voltammetry:

CV of fabrication step of AuNPl/ITO electrodes: Each modification step was analyzed by CV using $[Fe(CN)_6]^{3-}/[Fe(CN)_6]^{4-}$ as the redox probe. The prepared electrode was used as the working electrode, platinum wire acts as the counter electrode and saturated Ag/AgCl as the reference electrode in PBS (50mM, 0.9% NaCl, pH 7). The CV was carried out at a scan rate of 100m V/S from -0.4V to 0.8V. Distinct oxidative and reductive peaks were obtained despite of the amendments done on the electrode. Oxidation and reduction peaks obtained for gold nanopellets (Figure 3c) are at a more positive potential (0.48V and -0.18V respectively) as compared to the Au seed nanoparticles (Figure 3b) whose oxidation and reduction peaks are at lower positive potential (0.45V and -0.13V respectively). A peak current intensity of 1.357×10^{-4}A is observed for the bare ITO electrode (Figure 3a) being an electrically conductive material. An increase in the peak current is seen on deposition of Au seeds onto ITO due to the highly conducting properties of the gold. The peak current intensity of 4.417×10^{-4}A is observed for Au seeds (Figure 3b) whereas a peak current intensity of 5.215×10^{-4}A is recorded for AuNPl/ITO electrodes (Figure 3c). Apparently, the rise in peak current from Au seed coated ITO electrode to AuNPl/ITO electrode is not very high due to the presence of organic shape directing agent, CTAB. Anyways, sharp corners on the AuNPl are the location of electron confinement. Moreover, the peak separation of the Au seeds/ITO and AuNPl/ITO observed at 592mV and 668mV displays the feature of a reversible reaction on the electrodes.

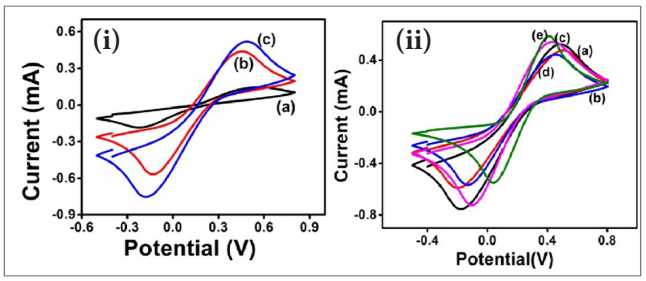

Figure 3: (i) CV of a) Bare ITO electrode b) Au seed/ITO and c) AuNPl/ITO at a scan rate of 100mV/S within a potential -0.4V to 0.8V in PBS buffer containing $Fe(CN)6^{3-/4-}$. (ii) CV of immunoelectrode at each modification step showing a) AuNPl/ITO b) Cys/AuNPl/ITO c) aOTA/Cys/AuNPl/ITO and d) BSA/aOTA/Cys/AuNPl/ITO (e) OTA/ BSA/aOTA/Cys/AuNPl/ITO at a scan rate of 100m V/S within a potential -0.4V to 0.8V in PBS buffer containing $Fe(CN)6^{3-/4-}$.

CV of immunoelectrode (BSA/aOTA/Cys/AuNPl/ITO): Cyclic voltammetry was performed at each immobilization step using the same redox probe and maintaining the same voltammetric conditions. Due to the insulating nature of the cystamine, the voltammogram of the cystamine functionalized electrode (Cys/AuNPl/ITO) shows smaller oxidation-reduction currents and a marginal shift in potential as compared to nanopellets with an observed peak current of 4.402×10^{-4}A (Figure 3ii-a). EDC-NHS is used to activate the antibody. EDC-NHS activation allows for linker less immobilization of antibodies over amine functionalized OTA electrode. The immobilization of activated aOTA onto the Cys/AuNPl/ITO electrode results in an increase in the peak current intensity to 5.410×10^{-4}A (Figure 3ii-d) because of the polar groups such as carboxyl and amine functionalities present on the activated antibody. Bovine Serum Albumin (BSA) is used to block the unwanted reaction sites at the electrode surface

hence inhibiting any non-specific reaction that could take place. The cyclic voltammogram of the BSA functionalized immunoelectrode (BSA/aOTA/Cys/AuNP/ITO) shows a peak current intensity of 4.753 × 10^{-4}A (Figure 3ii-b) which is less than the voltammogram shown by the immunoelectrode. This may be attributed to the presence of insulating protein macromolecules which in turn obstruct the acquiesce of ferrocene ions resulting in current plummet and a peak potential shift to a higher value [27]. On the contrary, the interaction with OTA and BSA/aOTA/Cys/AuNP/ITO immunoelectrode further enhances the current (Figure 3ii-e) which is attributed by the electrostatic interaction between paratope of a OTA and epitope of OTA. Figure 4 shows the schematic illustration of the fabrication steps of BSA/aOTA/Cys/AuNP/ITO immunoelectrode.

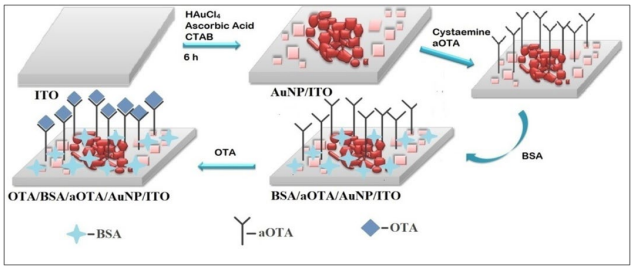

Figure 4: Schematic illustration of the stepwise of fabrication of BSA/aOTA/Cys/AuNPl/ITO immunoelectrode. (a) Bare ITO (b) AuNP1/ITO (c) aOTA/Cys/AuNP1/ITO (d) BSA/aOTA/Cys/AuNP1/ITO (e) OTA/BSA/aOTA/Cys/AuNP1/ITO.

Operational parameters of BSA/aOTA/Cys/AuNPl/ITO immunosensor

Operational parameters of fabricated immunoelectrode were examined by variation of antibody concentration (aOTA), cystamine concentration, the incubation time for antibody (aOTA) and antigen (OTA) interaction and operational pH. The optimum concentration of aOTA is found to be as 40ng mL^{-1} showing the maximum interaction between of BSA/aOTA/Cys/AuNPl/ITO electrodes and OTA for an incubation time of 35min. All the response studies are carried out at optimized pH 7.4 for which maximum interaction between BSA/aOTA/Cys/AuNPl/ITO electrodes and OTA is observed as determined by the peak current intensity as seen in figure 5c.

Response studies of the immunosensor

The response study of BSA/aOTA/Cys/AuNPl/ITO immunoelectrode was analyzed with CV measurements in PBS (pH 7.4) containing $[Fe(CN)_6]^{3-/4-}$ within a potential window of -0.4V to 0.8V at a scan rate of 100mV/S as a function of OTA concentration (1-20pg mL^{-1}). The immuno interaction between OTA and aOTA increases the polarity of the medium and helps to transport $[Fe(CN)_6]^{3-/4-}$. It is observed that the magnitude of current increases with the increase in concentration of OTA over the BSA/aOTA/Cys/AuNPl/ITO immunoelectrode. It can be noted that the anisotropic AuNPl affects the interaction of OTA with the immunoelectrode. Figure 5a shows the calibration curve of the OTA concentration with anodic peak current. The sensitivity of immunosensor is 2.89 × 10^{-5}Apg^{-1} mLcm^{-2} and LOD of 0.6pg mL^{-1} as obtained from the calibration curve (Figure 5a). The calibration curve (Figure 5a) shows a linear range of 1 to 20ng mL^{-1} with a regression-coefficient of (R^2=0.98). The association constant (K_a) obtained as 1.3mM is calculated using a Line Weaver-Burke Plot. The value of K_a indicates decent affinity of OTA towards the BSA/aOTA/Cys/AuNPl/ITO immunosensor due to favorable orientation of aOTA on the modified surface of ITO. The uniqueness of the presently developed OTA immunoelectrode is detection range falling in the pico gm range. However, four major points can be surmised, e.g., (i) unique shape and size of AuNPl crystal randomly sprayed over APTMS treated ITO surface, able to provide high surface area and electron confinement. The presence of sharp edges and corners enhances the number of active surface sites in anisotropic AuNPs compared to spherical AuNPs. The shape of a NPl is composed of a particular crystallographic plane, which ultimately determines the number of active surface sites present in that NPl. For example, with 5nm tetrahedral PtNPs, which have only {1,1,1} facets, 35% of the surface atoms are located at corners or edges, whereas this proportion is only 6% for cubes, with {1,0,0} facets. (ii) immobilization of very low concentration of aOTA (40ng mL^{-1}), (iii) amine functional group of Cys covalently binds with Fc part of aOTA to project Fab part of aOTA towards antigen to have optimum interaction, (iv) aOTA is attached through a small linker Cys molecule, imparts a direct linking of aOTA on electrode. The regression equation obtained on plotting anodic peak current vs. concentration (pg mL^{-1}) is represented by

$I=1.48 \times 10^{-4} \times 7.50 \times 10^{-6}C$, where I=current, C=concentration (1)

The repeatability of the BSA/aOTA/Cys/AuNPl/ITO immunosensor is confirmed by measuring the same sample by five times and then the Relative Standard Deviation (RSD) is calculated. A 4.2% of RSD for the repeated measurement of the same sample demonstrates a good repeatability of the electrochemical immunosensor.

Minimal interference is observed due to the presence of monoclonal antibody while testing in OTA spiked coffee extract. Table 1 distinguishes the results with Relative Error (% RE). The relative error was found to be in the range of 14.5%. The error % is attributed to extremely low concentration of OTA (in the pico gram range). Table 2 shows the characteristics of our developed immunosensor and some latest sensors developed for the detection of OTA. A comparative study with the reported literature clearly indicates that the presently developed electrode exhibits an abnormally low detection limit and entire detection range lies within the pico gram range.

Sample No.	Actual Spiked Concentration (pg/mL)	Experimental Concentration (pg/mL)	% Relative Error (% RE)
1	20	17.1	14.5
2	16	15.3	4.8
3	5	5.6	12

Table 1: Detection of OTA in spiked coffee extract.

Shelf life of BSA/aOTA/Cys/AuNPl/ITO immunoelectrode

The developed BSA/aOTA/Cys/AuNPl/ITO immunoelectrodes shows a good stability up to 20 days. Signal variation of 9.377% is obtained after 10 days assessment period (Figure 5b). Signal variation of 31% is obtained after 20 days assessment period. Thus, the developed electrode is stable up to 20 days. Low stability is due to the unstable nature of aOTA. Figure 5b shows the shelf life study of the immunoelectrode. Unique optimal conditions (pH, temperature, preservatives like sucrose and glycerol) for storage are important for antibodies in order prevent aggregation. In the developed immunosensor such conditions other that temperature cannot be maintained as it can hinder other characteristics of the immunosensor.

S. No	Matrix	Detection Range	LOD	Senstivity	Reference
1	AptOTA-MBs/SPE	0.78-8.74ng mL^{-1}	0.07ng mL^{-1}		Bonel et al. [20]
2	OTA-AP graphene/SPE	0.05-2.5µg L^{-1}	0.40µg/kg^{-1}		Alarcon et al. [18]
3	DApt/MB	-	0.11ng mL^{-1}		Barthelmebs et al. [28]
4	4-CP/aOTA	1-20ng mL^{-1}	0.5ng mL^{-1}		Radi et al. [17]
5	aOTA/MNPSs/Au	0.01-5ng mL^{-1}	0.01ng mL^{-1}		Zamfir et al. [19]
6	MIP/MWCNT/GCE	0.050-1.0µM	0.004µM		Pacheco et al. [29]
7	ThiolatedaptOTA/Au	10^{-8}-10^{2}ng mL^{-1}			Cheng et al. [22]
8	aOTA/BSA/Au	2.5-100ng mL^{-1}			Badea et al. [30]
9	aOTA-peroxidase/MB/SPE	10-4-1,000ng L^{-1}			Vidal et al. [31]
10	anti-OTA/Protein-A/PSi	0.001-100ng/mL	4.4pg mL^{-1}	0.01-5ng/mL	Myndrul et al. [32]
11	Glass/ZnO-NRs/Protein-A/BSA/Anti-OTA	10-4-20ng mL^{-1}	10^{-2}ng mL^{-1}	0.1-1ng/mL	Viter et al. [33]
12	aOTA/AuNPl/ ITO	1-20pg mL^{-1}	0.6pg mL^{-1}	2.89 × 10-5Apg mL^{-1}	Present

Table 2: A comparative report from the literature on the various electrochemical sensors of OTA.

Note: AptOTA-OTA Aptamer; SPE-Screen Printed Electrode; DApt-DNA aptamer, MB-Magnetic Bead; BSA-Bovine Serum Albumin; CP-4-Carboxyphenyl; Psi-Porous Silicon.

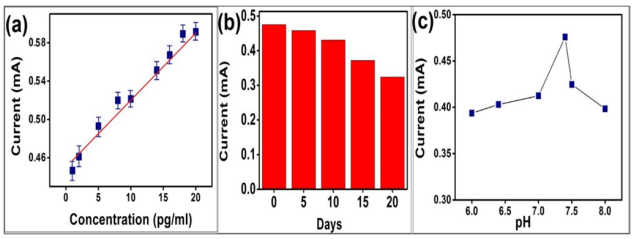

Figure 5: (a) Calibration curve obtained between the magnitudes of current (mA) versus concentration of aOTA (pg mL^{-1}). (b) Shelf life study of the immunoelectrode for a period of 20 days. (c) Effect of pH on Ipa of BSA/aOTA/Cys/AuNP1/ITO electrode.

Conclusion

In this work, a label free immunosensor is developed based on AuNPl for the ultra-low detection of OTA. The immunosensor exhibits a detection range of 1-20pg mL^{-1}, LOD of 0.6pg mL^{-1}, sensitivity of 2.89 × $10^{-5}$$Apg^{-1}$ $mLcm^{-2}$ and good association constant of 1.3mM is obtained.

The developed immunosensor is found to be highly propitious for ultra-low detection of OTA. AuNPl on ITO posses irregular geometry, indefinite shapes and sizes. The developed electrode is tunable and can be further modified to obtain a single morphology. Increasing the growth time to 18h-22h results in formation of gold nanorods. Preparation of nano rod also comprises various other shapes of nanopellet. The ultra low detection of OTA could be attributed by the anisotropic AuNPl, loading of very low concentration of a OTA and binding via Fc group with electrode surface to expose Fab part to expose towards OTA. The proposed electrode definitely promise high potential for application in ultra low detection of analyzes.

Acknowledgment

Authors gratefully acknowledge Inter University Accelerator Center, New Delhi for their support in characterizing the electrodes and materials which are developed in the present investigation.

References

1. Seo D, Park JC, Song H (2006) Polyhedra gold nanocrystals with O h symmetry: From octahedra to cubes. J Am Chem Soc 128: 14863-14870.
2. Li N, Zhao P, Astruc D (2014) Anisotropic gold nanoparticles : Synthesis, properties, applications, and toxicity. Angew Chem Int Ed Engl 53: 1756-1789.
3. Au L, Chen Y, Zhou F, Camargo PHC, Lim B, et al. (2008) Synthesis and optical properties of cubic gold nanoframes. Nano Res 1: 441-449.
4. Cobley CM, Xia Y (2010) Engineering the properties of metal nanostructures via galvanic replacement reactions. Materials Science and Engineering: R: Reports 70: 44-62.
5. He W, Henne WA, Wei Q, ZhaoY, Doorneweerd DD, et al. (2008) Two-photon luminescence imaging of Bacillus spores using peptide-functionalized gold nanorods. Nano Res 1: 450.
6. Mayorga-Martinez CC, Guix M, Madrid RE, Merkoçi A (2012) Bimetallic nanowires as electrocatalysts for nonenzymatic real-time impedancimetric detection of glucose. Chem Commun 48: 1686-1688.
7. Nandini S, Nalini S, Reddy MBM, Suresh GS, Melo JS, et al. (2016) Synthesis of one-dimensional gold nanostructures and the electrochemical application of the nanohybrid containing functionalized graphene oxide for cholesterol biosensing. Bioelectrochemistry 110: 79-90.
8. Pohland AE, Nesheim S, Friedman L (1992) Ochratoxin A: A review. Pure & Appl Chem 64: 1029-1046.
9. Petzinger E, Weidenbach A (2002) Mycotoxins in the food chain: The role of ochratoxins. Livestock Production Science 76: 245-250.
10. Fernández-Cruz ML, Mansilla ML, Tadeo JL (2010) Mycotoxins in fruits and their processed products: Analysis, occurrence and health implications. Journal of Advanced Research 1: 113-122.
11. Turner NW, Subrahmanyam S, Piletsky SA (2009) Analytical methods for determination of mycotoxins: A review. Anal Chim Acta 632: 168-180.
12. Yu FY, Vdovenko MM, Wang JJ, Sakharov IY (2011) Comparison of enzyme-linked immunosorbent assays with chemiluminescent and colorimetric detection for the determination of ochratoxin A in food. J Agric Food Chem 59: 809-813.
13. Chauhan R, Singh J, Sachdev T, Basu T, Malhotra BD (2016) Recent advances in mycotoxins detection. Biosens Bioelectron 81: 532-545.

14. Chauhan R, Singh J, Solanki PR, Manaka T, Iwamoto M, et al. (2016) Label-free piezoelectric immunosensor decorated with gold nanoparticles: Kinetic analysis and biosensing application. Sensors and Actuators B: Chemical 222: 804-814.

15. Kaushik A, Arya SK, Vasudev A, Bhansali S (2013) Recent advances in detection of ochratoxin-A. Open Journal of Applied Biosensor 2: 1-11.

16. Vidal JC, Bonel L, Ezquerra A, Hernández S, Bertolín JR, et al. (2013) Electrochemical affinity biosensors for detection of mycotoxins: A review. Biosens Bioelectron 49: 146-158.

17. Radi AE, Muñoz-Berbel X, Lates V, Marty JL (2009) Label-free impedimetric immunosensor for sensitive detection of ochratoxin A. Biosens Bioelectron 24: 1888-1892.

18. Alarcón SH, Palleschi G, Compagnone D, Pascale M, Visconti A, et al. (2006) Monoclonal antibody based electrochemical immunosensor for the determination of ochratoxin A in wheat. Talanta 69: 1031-1037.

19. Zamfir L, Geana I, Bourigua S, Rotariu L, Bala C, et al. (2011) Highly sensitive label-free immunosensor for ochratoxin a based on functionalized magnetic nanoparticles and EIS/SPR detection. Sensors & Actuators: B Chemical 159: 178-184.

20. Ngundi MM, Shriver-Lake LC, Moore MH, Lassman ME, Ligler FS, et al. (2005) Array biosensor for detection of ochratoxin a in cereals and beverages. Anal Chem 77: 148-154.

21. Bonel L, Vidal JC, Duato P, Castillo JR (2011) An electrochemical competitive biosensor for ochratoxin a based on a DNA biotinylated aptamer. Biosens Bioelectron 26: 3254-3259.

22. Cheng L, Qu H, Teng J, Yao L, Xue F, et al. (2017) Extraordinary tunable dynamic range of electrochemical aptasensor for accurate detection of ochratoxin a in food samples. Food Science and Human Wellness 6: 70-76.

23. Miranda A, Malheiro E, Eaton P, Carvalho PA, de Castro B, et al. (2011) Synthesis of gold nanocubes in aqueous solution with remarkable shape-selectivity. Journal of Porphyrins and Phthalocyanines 15: 441-448.

24. Xia Y, Xiong Y, Lim B, Skrabalak SE (2009) Shape-controlled synthesis of metal nanocrystals: Simple chemistry meets complex physics? Angew Chem Int Ed Engl 48: 60-103.

25. Sajanlal PR, Sreeprasad TS, Samal AK, Pradeep T (2011) Anisotropic nanomaterials: Structure, growth, assembly, and functions. Nano Rev 2.

26. Priecel P, Salami HA, Padilla RH, Zhong Z, Lopez-Sanchez JA (2016) Anisotropic gold nanoparticles: Preparation and applications in catalysis. Chinese Journal of Catalysis 37: 1619-1650.

27. Debgupta J, Pillai VK (2013) Thiolated graphene--a new platform for anchoring CdSe quantum dots for hybrid heterostructures. Nanoscale 5: 3615-3619.

28. Barthelmebs L, Hayat A, Limiadi AW, Marty JL, Noguer T (2011) Electrochemical DNA aptamer-based biosensor for OTA detection, using super paramagnetic nanoparticles. Sensors and Actuators B: Chemical 156: 932- 937.

29. Pacheco JG, Castro M, Machado S, Barroso MF, Nouws HPA, et al. (2015) Molecularly imprinted electrochemical sensor for ochratoxin a detection in food samples. Sensors and Actuators B: Chemical 215: 107-112.

30. Badea M, Floroian L, Restani P, Cobzac SC, Moga M (2016) Ochratoxin a detection on antibody- immobilized on BSA-functionalized gold electrodes. PLoS One 11: 0160021.

31. Vidal JC, Bonel L, Ezquerra A, Duato P, Castillo JR (2012) An electrochemical immunosensor for ochratoxin a determination in wines based on a monoclonal antibody and paramagnetic microbeads. Anal Bioanal Chem 403: 1585-1593.

32. Myndrul V, Viter R, Savchuk M, Shpyrka N, Erts D, et al. (2018) Porous silicon based photoluminescence immunosensor for rapid and highly-sensitive detection of Ochratoxin A. Biosens Bioelectron 102: 661-667.

33. Viter R, Savchuk M, Iatsunskyi I, Pietralik Z, Starodub N, et al. (2018) Analytical, thermodynamical and kinetic characteristics of photoluminescence immunosensor for the determination of Ochratoxin A. Biosens Bioelectron 99: 237-243.